Heteroepitaxial Growth of GaP/ZnS Nanocable with Superior Optoelectronic Response

Linfeng Hu,[†] Megan M. Brewster,[§] Xiaojie Xu,[†] Chengchun Tang,[‡] Silvija Gradečak,[§] and Xiaosheng Fang*[,†]

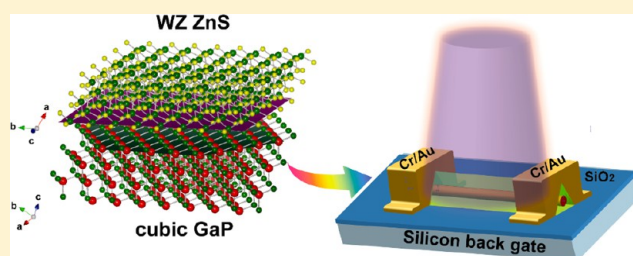[†]Department of Materials Science, Fudan University, Shanghai 200433, P. R. China

[‡]School of Materials Science and Engineering, Hebei University of Technology, Tianjin 300130, P. R. China

[§]Department of Materials Science and Engineering, Massachusetts Institute of Technology, 77 Massachusetts Avenue, Cambridge, Massachusetts 02139, United States

S *Supporting Information*

ABSTRACT: We demonstrate the controlled growth of coaxial nanocables composed of GaP/ZnS core−shell structures by a facile chemical vapor deposition method. Structural analysis confirms that the cubic GaP (111) plane and wurtzite ZnS (0001) plane present close similarities in terms of hexagonal-arranged atomic configuration with small in-plane lattice mismatch, and the ZnS shell is epitaxially grown on the (100) plane of the cubic GaP core. Compared with the unitary ZnS nanobelts, the GaP/ZnS coaxial nanocables exhibit improved optoelectronic properties such as high photocurrent and excellent photocurrent stability. This approach opens up new strategy to boost the performance of ZnS-based photodetectors.

KEYWORDS: *GaP/ZnS, nanocable, heteroepitaxial growth, optoelectronic response*

Semiconductor nanostructures, including nanowires, nanorods, and nanotubes, are important building blocks for constructing novel nanodevices.[1] In the past decade, great interest has been placed in novel electronic devices based on semiconductor nanostructures, such as silicon,[2] InP nanowires,[3] ZnO nanowire arrays,[4,5] ZnS nanobelts[6−8] and so forth. Among these functional nanomaterials, wide band gap ZnS nanostructures have been widely used in optoelectronic devices, such as photodetectors and light-emitting devices. For example, we have previously developed UV-A light sensors from individual ZnS nanobelts, but these optoelectronic devices suffer from low photocurrent and poor stability.[6,7] Therefore, enhancing the performance and device stability is required for the further development of ZnS nanostructure-based photodetectors.

The ability to control and modulate the composition, crystal structure, and morphology of nanostructures by rationally designing the synthesis process is critical for exploring various intriguing physical properties of nanomaterials.[9,10] In our earlier studies, we have successfully realized a series of semiconducting biaxial nanobelts and core−shell nanostructures consisting of several different functional materials with novel photoresponsive and optical properties, respectively.[11−14] However, only a limited number of reports focus on the optoelectronic properties of ZnS-based nanocomposites.[15] Since gallium phosphide (GaP) is an important group III−V semiconductor with an indirect band gap of 2.26 eV and has a great potential

for optoelectronic devices,[16] herein, we synthesize GaP/ZnS coaxial nanocables and use it to fabricate UV-light sensors. The detailed structure and growth mechanism of these GaP/ZnS coaxial nanocables has been clarified. Compared with the bare ZnS nanobelts, the GaP/ZnS coaxial nanocables exhibit superior optoelectronic properties.

We grew GaP/ZnS coaxial nanocables by a chemical vapor deposition method. Appropriate amounts of Ga_2O (0.28 g), P (0.11 g), carbon powders (0.02 g), and ZnS powder (0.36 g, purity: 99.99%) were mixed in an alumina boat and vacuum-sealed in a thick quartz capsule (see experimental details in Supporting Information). Silicon substrates coated with a 3-nm-thick Au layer were placed downstream of the source material. The tube furnace was heated to 1100 °C for 1−2 h while simultaneously supplying high-purity argon (Ar) at a flow rate of 100 sccm. After the furnace cooled down to room temperature, white-colored wool-like material was deposited onto the substrate surface. Figure 1a displays a low-magnification scanning electron microscopy (SEM) image of the product revealing the high density of the resulting nanowire-like structures with lengths of several tens of micrometers and diameter from several tens to several hundred nanometers. We found that most of the as-grown nanocables
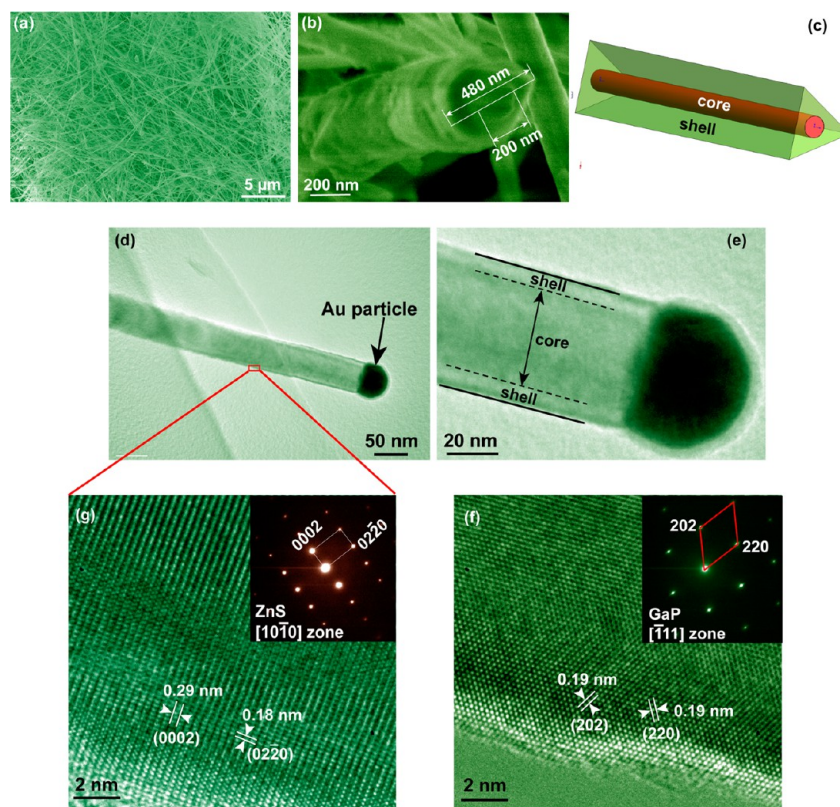
Figure 1. (a) Low- and (b) high-magnification SEM images of the as-grown GaP/ZnS coaxial nanocables. (c) A schematic illustration of the coaxial nanocable. (d) Low- and (e) high-magnification TEM image of an individual nanocable capped with a Au nanoparticle. HRTEM images taken from (g) main body and (f) end part of the nanocable, showing ZnS and GaP lattice fringes, respectively. The insets are the corresponding SAED patterns.
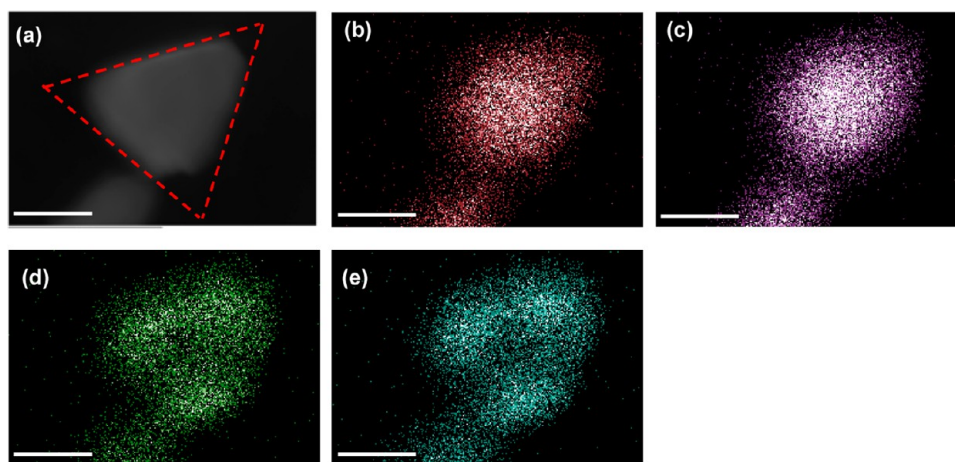
Figure 2. (a) A cross-sectional view of the as-grown nanocable and the corresponding EDS elemental mapping of (b) Ga, (c) P, (d) Zn, and (e) S elements. The scale bar is 200 nm.

(about 80% portion) consist of a cylinder core and a triangular prism shell, as typically shown in the high-magnification SEM image (Figure 1b). The diameter of the inner cylinder for the nanocable highlighted in Figure 1b is ∼200 nm, and the maximal diameter of the core/shell prism is ∼480 nm, approximately. A schematic view of the cable structure is shown in Figure 1c. Transmission electron microscopy (TEM) observation from a thinner nanocable also confirms the core–shell structure, as shown in Figure 1d and e. An Au nanoparticle was clearly visible at the tip of the nanocable. High-resolution transmission electron microscopy (HRTEM) images in Figure 1g were taken from the domain labeled by a rectangle in Figure

1d, exhibiting two-dimensional (2D) lattice fringe of wurtzite (WZ) ZnS, implying that the shell of nanocable is composed of crystalline ZnS. The 0.29 and 0.18 nm spacing of the lattice fringes agrees well with the (0002) and (02−20) plane of WZ ZnS. The inset of Figure 1e shows the corresponding selected area electron diffraction (SAED) pattern. The sharp diffraction plots reveal a single crystalline nature, which can be indexed to the expected [10−10] zone-axis of WZ ZnS. Note that no diffraction spots from the GaP phase were observed in this SAED pattern. This result is quite different with the SAED patterns of ZnO/SnO$_2$ core−shell nanotetrapods reported by another group, in which two sets of diffraction patterns
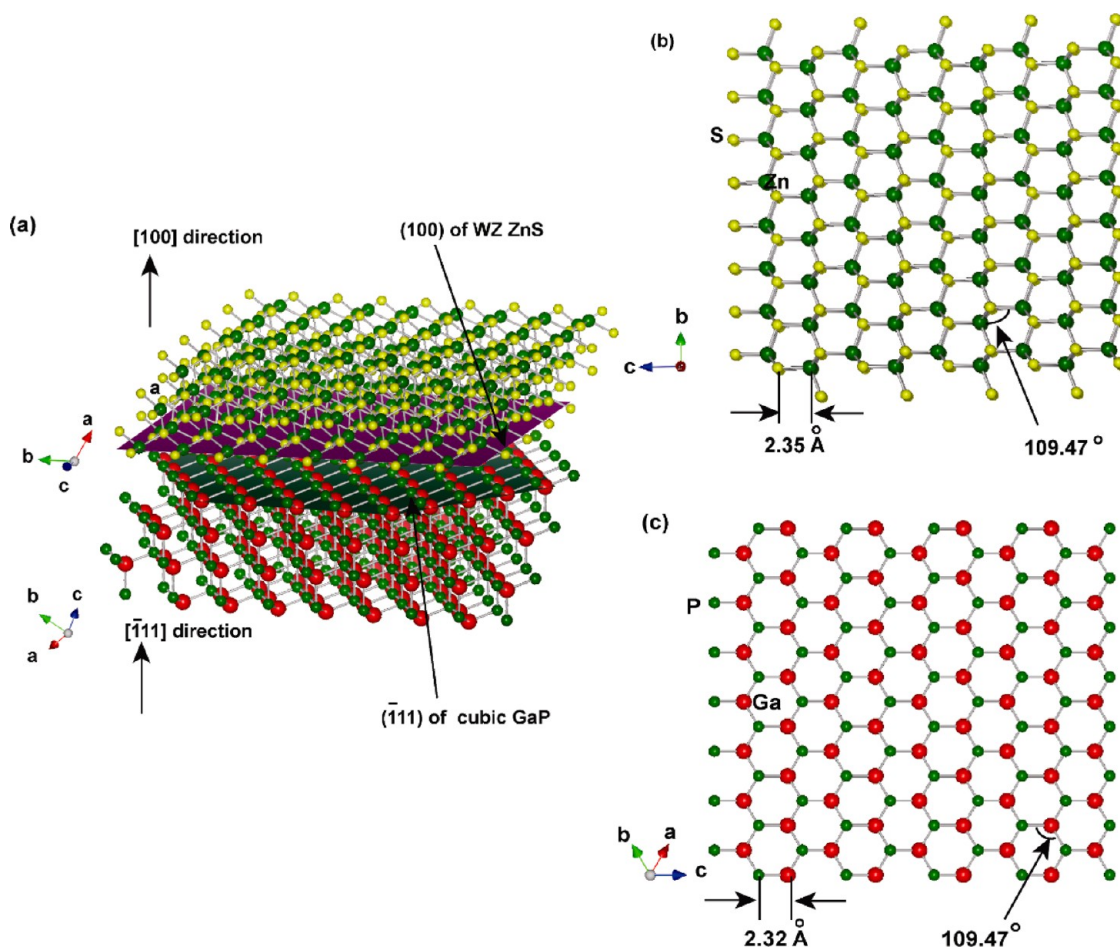
Figure 3. (a) Schematic illustration of epitaxial growth of [100] oriented ZnS shell on the GaP (111) plane. Top-view atomic structures of epitaxial (b) WZ ZnS (100) plane and (c) GaP (111) plane.

respectively originated from the core and shell coexists.[17] The absence of GaP diffraction spots in the main body of the nanocable should be attributed to the fact that the radiation area of incident electron beam does not cover the inner GaP core during the observation. We further checked the SAED pattern taken from the end part of this nanocable. As shown in Figure 1f, the hexagonally arranged sharp diffraction spots can be indexed into the [−111] zone axis pattern of cubic GaP. The absence of ZnS diffraction spots in the end part implies that the end of this nanocable (not shown here) is only composed of the exposed GaP phase. The corresponding HRTEM image in Figure 1f displays a clear two-dimensional lattice fringe. The 0.19 nm spacing corresponds closely to the {220} planes of the cubic GaP. Note that the nanocable in Figure 1b displays a rather rough surface. In fact, a smooth surface such as the one shown in Figure 1d has been frequently observed for most of the nanocables, demonstrating high crystallinity of our products.

To further verify the component and structure of the resulting core−shell nanocable, bright-field scanning transmission electron microscope (STEM) studies were performed. Figure 2a shows the cross-sectional TEM image of the nanocable, very consistent with the SEM observation (Figure 1b). The corresponding energy dispersive X-ray spectroscopy (EDS) mapping data in Figure 2b−e confirms that the Ga and P are homogeneously distributed within the core part and that the Zn and S spread in the shell part. The core−shell structure

of the nanocable is also confirmed by the line-scanning elemental maps taken along the radial direction as shown in Figure S2. It is clear that Zn and S elements are abundant from the side-part of the nanocable, and the center of cable mainly consists of Ga and P elements. Furthermore, from the EDS mapping from a planar view nanocable in Figure S3, one can clearly see that the core contains only Ga and P, while the shell consists of only Zn and S. Together with TEM results, these results demonstrate that the as-grown nanocables consist of a cubic GaP cylinder core and a WZ ZnS prism shell. The aforementioned SAED patterns inserted in Figure 1g and f suggest that the ZnS shell is grown nonuniformly along the axial direction of the nanocable, and the end part of the cable is only composed of exposed GaP core. This was further demonstrated by the EDS mapping taken from the end part of a nanocable. As shown in Figure S4, the nanocable exhibits a caudal end composed of a well-defined GaP core and a broken ZnS shell with insufficient Zn and S elements.

The growth mechanism of this novel GaP/ZnS coaxial nanocable is investigated in detail. Due to the much lower melting point (T_m) of GaP (∼1730 K) than that of ZnS (2103 ± 20 K), GaP may grow first prior to the crystallization of ZnS phase during the evaporation process.[18] According to our early studies,[19] the formation of GaP phase can be expressed by the following reaction:

$$Ga_2O_{(g)} + C + 2P_{(g)} \xrightarrow{1100\,°C} 2GaP + CO_{(g)}$$
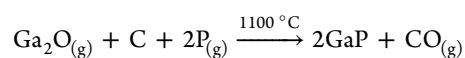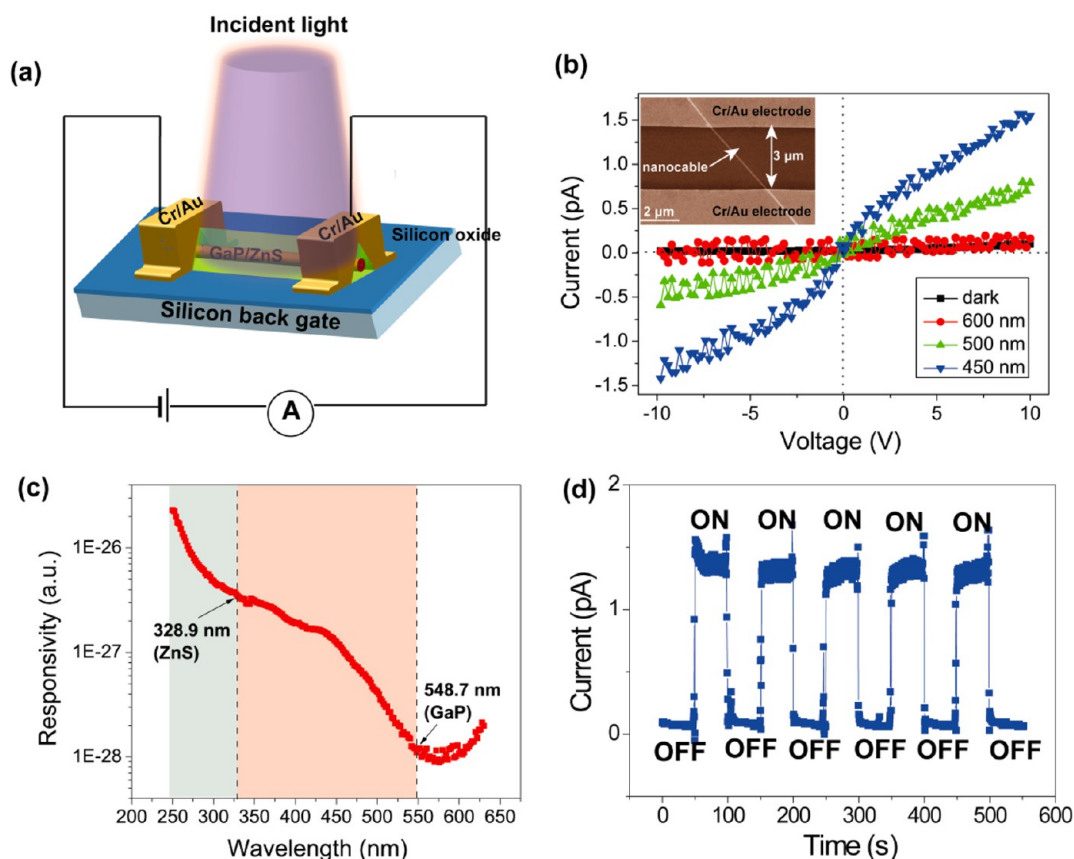
Figure 4. (a) Schematic three-dimensional structure of a photodetector constructing from an individual GaP/ZnS coaxial nanocable. (b) Current−voltage (I−V) characteristics of the GaP/ZnS nanocable photodetector illuminated with 450−600 nm light and under dark conditions. Inset shows a typical SEM image of the device. (c) Spectral photoresponse measured from the UV-light device at a bias of 10.0 V. (d) The reproducible on/off switching upon 450 nm light illumination at a bias of 10.0 V.

The presence of Au nanoparticle at the tip of each nanocable indicates that the nanocable may be grown by a conventional vapor−liquid−solid (VLS) model.[20,21] Since the T_m of ZnS is much higher than the growth temperature in the present study, it is rational that the GaP core grows via VLS mechanism by incorporating with Au particle rather than the ZnS shell. Accordingly, during the first stage, GaP vapors are continuously transferred to the low-temperature zone and deposited on the silicon substrates coated with Au layer. The Au catalysis layer then forms a eutectic liquid nanodroplet with the Ga and P atoms, and the supersaturation of the Ga and P atoms leads to homogeneous nucleation of a GaP 1D single crystalline nanowire. Subsequently, ZnS powder was evaporated with assistance of Ar flow in the high temperature zone to form ZnS vapor and eventually deposited on the as-formed GaP core to form a ZnS shell, leading to a coaxial GaP/ZnS nanocable structure.

The as-observed SAED patterns for GaP core and ZnS shell are indexed to the $[-111]$ and $[10-10]$ zone axes, respectively. Therefore, the exposed crystal plane of the GaP core and ZnS shell should be (111) plane for GaP and (0001) plane for ZnS, and the crystallographic orientation relationship can be identified as: $(111)_{GaP}//(0001)_{ZnS}$ and $[-111]_{GaP}//[10-10]_{ZnS}$. One may speculate that the (0001) plane of ZnS was epitaxially grown on the (111) plane of GaP which is illustrated in Figure 3c. Structurally, the present GaP and ZnS belong to two different crystal systems, the cubic crystal structure with a = 5.35 Å (space group: $F-43m$) and the hexagonal wurtzite

structure with a = 3.82 Å, c = 6.26 Å, and γ = 120° (space group: $P63mc$) (see Figure S1). It seems that there should be a striking difference between the two types of structures, and it is difficult to grow such a GaP/ZnS nanocable with an epitaxial relation. Although a cubic structured ZnS layer has been epitaxially grown on cubic GaP substrate due to the nearly lattice-match, there has been no report about the epitaxy of hexagonal WZ ZnS on cubic GaP.[22] By carefully analyzing both crystal structures, we found the possibility of heteroepitaxial growth of the crystalline ZnS shell on the GaP core. Top-view structures of cubic GaP (111) plane and WZ ZnS (0001) plane are depicted in Figure 3d and e, respectively. One can note that these two planes present close similarities in terms of hexagonal-arranged atomic configuration. In GaP (111) plane, the Ga−P bond distance is 2.32 Å with P−Ga−P angle of 109.47°. In WZ ZnS (100) plane, the Zn−S bond distance is 2.35 Å, and Zn−S—Zn shows an equivalent angle of 109.47°. Therefore, the in-plane lattice mismatch between WZ ZnS and cubic GaP can be estimated to be as small as $(d_{ZnS} - d_{GaP})/d_{GaP}$ = 1.29%. This structural compatibility provides important evidence that WZ ZnS shell was planar epitaxially grown on the GaP core via the vapor−solid mechanism: $GaP + ZnS \xrightarrow{1100\,°C} GaP_{(core)}/ZnS_{(shell)}$.[23] Furthermore, since the GaP (111) plane and ZnS (100) plane respectively show spacing of 3.07 Å and 3.27 Å, the out-plane mismatch along the $[-111]_{GaP}$ and $[100]_{ZnS}$ is relatively large, and thus some misfit dislocations may exist in order to release the strain.

Table 1. An Overview of Dark Current, Photocurrent, and External Quantum Efficiency (EQE) of the Photodetectors Constructed from Pure ZnS Nanostructure and GaP/ZnS Nanocables

photodetectors		amount of nanostructures	dark current	photocurrent (at 10.0 V)	reference
ZnS nanobelt (diameter: ~300 nm)		individual	0.07 pA	0.8 pA (320 nm)	6
				$\ll$ 0.1 pA (450 nm)	
GaP/ZnS nanocable (diameter: ~100 nm)	Device 1	individual	0.05 pA	1.55 pA (450 nm)	this work
	Device 2	two	0.06 pA	3.28 pA (450 nm)	
	Device 3	several	0.15 pA	5.03 pA (450 nm)	
	Device 4	multiple	0.89 pA	10.56 pA (450 nm)	
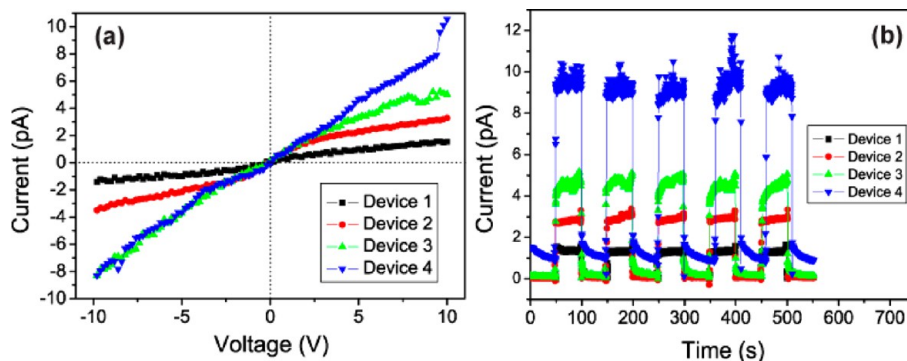
Figure 5. (a) $I-V$ curves of the Devices 1−4 upon 450 nm light illumination. (b) The corresponding time response at a bias of 10.0 V.

The high crystallinity, well-defined geometry shape, well-ordered crystallographic orientation, and high surface-volume-ratio of the as-grown nanocables should be beneficial for optoelectronic and microelectronic applications. For that reason, we next investigated the photoresponse behavior of the GaP/ZnS coaxial nanocables. As illustrated in Figure 4a, a pair of 3 μm spaced Cr/Au electrodes (10 nm/100 nm) was deposited on a GaP/ZnS coaxial nanocable with a diameter of ~100 nm dispersed at a SiO$_2$/Si substrate by standard lithography procedures to form a top-contacted device. $I-V$ measurements were performed on this device by a two-probe method under ambient air conditions. As shown in Figure 4b, the photocurrent under illumination of a 600 nm light exhibits no apparent increase compared with that obtained in the dark (0.1 pA). However, it increases to 0.79 pA under 500 nm light illumination (2.81 mW cm^{-2}) and further to 1.55 pA under 450 nm light illumination (2.80 mW cm^{-2}) at an applied voltage of 10.0 V. The increase of photoconductive sensitivity is ascribed to the electron−hole pairs excited by the incident photons with energy larger than the band gap. The approximately symmetric and linear $I-V$ curves indicate the ohmic contact of the GaP/ZnS nanocable with the Cr/Au electrodes. This ohmic characteristic is quite different from the rectification curves which are usually observed in some nanowire heterojunction-based photodetectors, suggesting that no photogenerated carriers are trapped and blocked at the present GaP/ZnS interface of the core−shell nanocable.[24,25]

Figure 4c displays the spectral photoresponse of the device at a bias of 10.0 V at different wavelengths from 250 to 630 nm. The sensitivity is relatively low when the wavelength is higher than 550 nm and gradually increases by about 2 orders of magnitude when the device is illuminated by a light with energy above this threshold wavelength. Such a result is obviously different from that obtained from a pure ZnS nanobelt in our previous study, for which the threshold wavelength is 320 nm. Note that GaP is a compound semiconductor material with an indirect band gap of 2.26 eV and a direct band gap of 2.78 eV at

300 K. GaP begins to absorb incident light at a wavelength shorter than 548.7 nm, and the adsorption increases strongly as the photon energy increases past the direct band gap about 450 nm. Therefore, the spectral photoresponse in Figure 4c demonstrates that the incident light can penetrate the ZnS shell due to its thinness of ~40 nm and excite electron−hole pairs in semiconducting GaP core. The dark photocurrent of the present device is comparable with that of the pure ZnS nanobelt based device in our early study.[6] It is also noteworthy that the diameter of present GaP/ZnS nanocable is much smaller than that of pure ZnS nanobelt (see Table 1). However, the photocurrent of GaP/ZnS nanocable is two times higher than that of pure ZnS nanobelt-based device measured at the same conditions. Generally, thinner 1D nanostructures would absorb less light due to their smaller surface and thus generate lower photocurrent. Therefore, the superior photoresponse behavior by using the GaP/ZnS nanocable as the building block of the nanodevice should be due to some intrinsic physical mechanism rather than the size effect. We speculate that one of the reasons might be due to the fact that optoelectronic signal of our present devices is integrated from both GaP core and ZnS shell. The band diagram of the present GaP/ZnS heterostructred nanocable is schematically depicted in Figure S5 according to the previous reports from other groups.[26] A straddling band alignment is formed, where at the hetero-junction both the valence and conduction band edges of the GaP core are localized within the energy gap of the ZnS shell.[27] Since the ZnS shell has higher band gap than the GaP core, at first glance it seems that the photogenerated carriers in the GaP core may be confined in the narrow energy region and hardly transfer to the ZnS shell and then to the electrodes. However, note that the end of this nanocable is only composed of the exposed GaP phase as confirmed in Figure 1f. Accordingly, a pair of Au/Cr electrodes might contact the ZnS shell on one side and also the GaP core on another side. The photo-generated carriers in the GaP core might directly transfer to the

Au/Cr electrodes, leading to an enhanced photocurrent of the device.

Repeatability and response speed are key parameters which determine the ability of a photodetector under a quickly varying optical signal. Figure 4d reveals the time response of the device is faster than the limit of our measurement setup (0.3 s). No abrupt degradation of the device was detected after several tens of on/off switching cycles. Compared with the jagged current–time characteristic obtained from the pure ZnS nanobelt report previously, the stability of the present GaP/ZnS nanocable photodetector is significantly enhanced.

The performance of the GaP/ZnS nanocable photodetector can be further improved using multiple GaP/ZnS nanocables. Figure S6 shows the four kinds of devices constructed from different amount of the nanocables, which were denoted as Devices 1–4, respectively. The optoelectronic performance of these devices is shown in Figure 5 and summarized in Table 1. By increasing the amount of nanocables, the photocurrent of the devices gradually increase up to 10.56 pA, about 10 times enhancement compared with the individual nanocable-based device has been detected. Furthermore, the response time <0.3 s and excellent photocurrent reproducibility are also evident in Figure 5b for these devices. Note that the OFF current of Device 4 does not return to the same level as the OFF current of Device 1–3. The real reason for this result is still not so clear, but we speculate that it might be attributed to the prominent trapping effect of the photogenerated holes when the amount of nanocable is highly increased for Device 4. This trapping effect slows down the recombination with the free electrons and increases the majority carrier lifetime.[28]

In summary, we have successfully grown GaP/ZnS core–shell coaxial nanocables with well-defined morphology by a facile chemical vapor deposition route. The WZ ZnS shell is epitaxially grown on the (100) plane of the cubic GaP core. A photodetector constructed from the GaP/ZnS nanocables showed higher photocurrent and much better stability compared with the bare ZnS nanostructure. The present study may open a facile strategy to improve the optoelectronic performance of ZnS-based photodetectors, and this strategy may be extended to grow some other core–shell nanostructures.

■ ASSOCIATED CONTENT

Ⓢ Supporting Information

Details for preparation and characterizations of samples, crystal structures, EDS mapping, and band alignment of the nanocables. This material is available free of charge via the Internet at http://pubs.acs.org.

■ AUTHOR INFORMATION

Corresponding Author
*E-mail: xshfang@fudan.edu.cn.

Present Address
M.M.B.: GE Global Research, 1 Research Circle, Niskayuna, NY 12309.

Notes
The authors declare no competing financial interest.

■ ACKNOWLEDGMENTS

■ REFERENCES

(1) Lieber, C. M. *MRS Bull.* **2011**, *36*, 1052−1063.
(2) Cui, Y.; Wei, Q.; Park, H.; Lieber, C. M. *Science* **2001**, *293*, 1289−1292.
(3) Wang, J. F.; Gudiksen, M. S.; Duan, X. F.; Cui, Y.; Lieber, C. M. *Science* **2001**, *293*, 1455−1457.
(4) Law, M.; Greene, L. E.; Johnson, J. C.; Saykally, R.; Yang, P. D. *Nat. Mater.* **2005**, *4*, 455−459.
(5) Wang, X. D.; Song, J. H.; Liu, J.; Wang, Z. L. *Science* **2007**, *316*, 102−105.
(6) Fang, X. S.; Bando, Y.; Liao, M. Y.; Gautam, U. K.; Zhi, C. Y.; Dierre, B.; Liu, B. D.; Zhai, T. Y.; Sekiguchi, T.; Koide, Y.; Golberg, D. *Adv. Mater.* **2009**, *21*, 2034−2039.
(7) Fang, X. S.; Bando, Y.; Liao, M. Y.; Zhai, T. Y.; Gautam, U. K.; Li, L.; Koide, Y.; Golberg, D. *Adv. Funct. Mater.* **2010**, *20*, 500−508.
(8) Likovich, E. M.; Jaramillo, R.; Russel, K. J.; Ramanathan, S.; Narayanamurti, V. *Adv. Mater.* **2011**, *23*, 4521−4525.
(9) Tian, B. Z.; Xie, P.; Kempa, T. J.; Bell, D. C.; Lieber, C. M. *Nat. Nanotechnol.* **2009**, *4*, 824−829.
(10) Tian, B. Z.; Zheng, X. L.; Kempa, T. J.; Fang, Y.; Yu, N. F.; Yu, G. H.; Huang, J. L.; Lieber, C. M. *Nature* **2007**, *449*, 885−890.
(11) Hu, L. F.; Liao, M. Y.; Xiang, H. J.; Gong, X. G.; Zhang, L. D.; Fang, X. S. *Adv. Mater.* **2012**, *24*, 2305−2309.
(12) Yan, J.; Fang, X. S.; Zhang, L. D.; Bando, Y.; Gautam, U. K.; Dierre, B.; Sekiguchi, T.; Golberg, D. *Nano Lett.* **2008**, *11*, 5316−5321.
(13) Qian, F.; Brewster, M.; Lim, S. K.; Ling, Y. C.; Greene, C.; Laboutin, O.; Johnson, J. W.; Gradečak, S.; Cao, Y.; Li, Y. *Nano Lett.* **2012**, *12*, 3344−3350.
(14) Lim, S. K.; Crawford, S.; Haberfehlner, G.; Gradečak, S. *Nano Lett.* **2013**, *13*, 331−336.
(15) Wei, D. C.; Liu, Y. Q.; Cao, L. C.; Zhang, H. L.; Huang, L. P.; Yu, G. *Chem. Mater.* **2010**, *22*, 288−293.
(16) Levinshtein, M.; Rumyantsev, S.; Shur, M. *Handbook Series on Semiconductor Parameters*; World Scientific: London, 1996; Vol. *1*, pp 104−124.
(17) Kuang, Q.; Jiang, Z.-Y.; Xie, Z.-X.; Lin, S.-C.; Lin, Z.-W.; Xie, S.-Y.; Huang, R.-B.; Zheng, L.-S. *J. Am. Chem. Soc.* **2005**, *127*, 11777−11784.
(18) Addamiano, A.; Dell, P. A. *J. Phys. Chem.* **1957**, *61*, 1020−1021.
(19) Tang, C. C.; Fan, S. S.; Chapelle, M. L.; Dang, H. Y.; Li, P. *Adv. Mater.* **2000**, *12*, 1346−1348.
(20) Weert, M. H. M.; Helman, A.; Einden, W. V. D.; Algra, R. E.; Verheijen, M. A.; Borgström, M. T.; Immink, G.; Kelly, J. J.; Kouwenhoven, L. P.; Bakkers, E. P. A. M. *J. Am. Chem. Soc.* **2009**, *131*, 4578−4579.
(21) Lin, P. A.; Liang, D.; Reeves, S.; Gao, X. P. A.; Sankaran, R. M. *Nano Lett.* **2012**, *12*, 315−320.
(22) Bertóti, I.; Farkas-Jahnke, M.; Lendvay, N. *J. Mater. Sci.* **1969**, *4*, 699−703.
(23) Jiang, Y.; Meng, X. M.; Liu, J.; Xie, Z. Y.; Lee, C. S.; Lee, S. T. *Adv. Mater.* **2003**, *15*, 323−327.

(24) Lin, H. W.; Liu, H. B.; Qian, X. M.; Lai, S.-W.; Li, Y. J.; Chen, N.; Ouyang, C.; Che, C.-M.; Li, Y. L. *Inorg. Chem.* **2011**, *50*, 7749−7753.

(25) Han, Y. G.; Fan, C. C.; Wu, G.; Chen, H.-Z.; Wang, M. *J. Phys. Chem. C* **2011**, *115*, 13438−13445.

(26) Landis, G. A.; Loferski, J. J.; Beaulieu, R.; Sekula-Moisé; Vernon, S. M.; Spitzer, M. B.; Keavney, C. J. *IEEE Trans. Dev.* **1990**, *37*, 372−381.

(27) Lo, S. S.; Mirkovic, T.; Chuang, C.-H.; Burda, C.; Scholes, G. D. *Adv. Mater.* **2011**, *23*, 180−197.

(28) Amos, F. F.; Morin, S. A.; Streifer, J. A.; Hamers, R, J.; Jin, S. *J. Am. Chem. Soc.* **2007**, *129*, 14396−14302.